# DFT-based evaluation of $Li_2MnO_3$ as a promising cathode coating material for lithium-ion batteries

**Mogau Kgasago[1], Katlego Phoshoko[2], Phuti Ngoepe[1], and Raesibe Ledwaba[1]**

[1]Materials Modelling Centre, University of Limpopo, Private Bag x1106 Sovenga, 0727, South Africa

[2]Data Intensive Research Initiative of South Africa, Council for Scientific and Industrial Research, P.O. Box 395, Pretoria, 0001, South Africa

E-mail: 201818190@myturf.ul.ac.za

**Abstract:** An ideal coating material should combine chemical stability, mechanical strength, and suitable conductivity to enhance cathode durability. $Li_2MnO_3$ has previously been used as a coating material due to its stabilizing effect on the core, but other beneficial properties it may offer as a coating material are still underexplored. In this study, these ideal coating properties of $Li_2MnO_3$ were investigated using Density Functional Theory (DFT). To enhance accuracy, spin configurations were also considered, and calculations were performed using the GGA+U functional. The findings show that $Li_2MnO_3$ is thermodynamically stable, mechanically robust, and a semiconductor with a band gap of 2.17 eV. These results affirm $Li_2MnO_3$ as a promising cathode coating material, possessing the key attributes which are thermodynamic, electronic, and mechanical stability needed to enable durable, high-performance lithium-ion battery systems.

## 1 Introduction

$LiMn_2O_4$ is a sustainable, affordable, and thermally stable alternative to cobalt-rich cathodes [1]. Its ability to accommodate extra lithium in octahedral sites makes it particularly attractive as a pre-lithiation agent. Prelithiation, which involves indirectly adding extra active lithium to the anode via the cathode, has emerged as a key solution to mitigate initial capacity losses in lithium-ion batteries [2]. Pre-lithiating pristine spinel $LiMn_2O_4$ (with an initial theoretical capacity of 147 mAh/g) can raise its capacity to 284 mAh/g [3]. However, this is still lower than that of layered oxides. The main limitations of $LiMn_2O_4$ arises from capacity loss caused by manganese (Mn) dissolution, the Jahn–Teller effect, and other degradation mechanisms [4]. Addressing these issues is essential before $LiMn_2O_4$ can be fully utilized as an effective pre-lithiation agent. Various strategies have been proposed to enhance the stability and performance of $LiMn_2O_4$. These include doping, surface coatings, and other surface modification techniques aimed at improving its structural integrity and electrochemical properties [5-7]. Among these, core–shell designs have shown particular promise. These designs retain the high-rate capability and capacity of the core while introducing a protective shell to improve structural stability [8]. For example, Tomon et al. developed a $LiMn_2O_4$@C core–shell structure that significantly improved battery performance [9]. The carbon shell helped minimize Mn loss, stabilized phase transitions, and maintained structural integrity during cycling, leading to enhanced cycling stability and longer lifespan compared to pristine $LiMn_2O_4$ [9]. However, despite these improvements, the incompatibility between the carbon shell and the oxide core causes interfacial phase separation over extended cycling, which eventually degrades the electrode's performance.

To overcome such compatibility issues, a more chemically and structurally compatible shell material is needed. Layered $Li_2MnO_3$ is a promising candidate due to its high lithium content, good thermal stability, and its ability to co-exist with $LiMn_2O_4$ [10]. These features make $Li_2MnO_3$ a suitable shell material for enhancing both the

stability and capacity of spinel-based core–shell cathodes. Unlike previous DFT studies that primarily evaluated $Li_2MnO_3$ as a coating material in isolation, this work uniquely examines its interaction with the $LiMn_2O_4$ spinel, giving insights into their structural and electronic compatibility. In this study, we use density functional theory (DFT) to systematically evaluate the structural and electronic compatibility of $Li_2MnO_3$ as a shell for $LiMn_2O_4$. By analyzing oxidation states, electronic density of states, and lithium-ion pathways, we aim to determine whether $Li_2MnO_3$ can effectively stabilize $LiMn_2O_4$ and support its application as a high-capacity cathode material.

## 2 Method

First-principles calculations based on Density Functional Theory (DFT**)** were performed using the Vienna Ab Initio Simulation Package (VASP 6.0) [11, 12]. The Generalized Gradient Approximation (GGA) with the Perdew-Burke-Ernzerhof (PBE) exchange-correlation functional [13] was used, along with the DFT+U approach [14] to correct for strong on-site Coulomb interactions in the Mn 3*d* orbitals. The Hubbard U parameter was set to 4 eV for $LiMn_2O_4$ and 5 eV for $Li_2MnO_3$, values benchmarked by testing several U inputs and selecting those that produced the lowest ground-state energies [14]. Total energy convergence tests were performed prior to all property calculations to ensure numerical accuracy. The Brillouin zone was sampled with a 5×5×5 k-point grid for $LiMn_2O_4$ and 4×4×4 for $Li_2MnO_3$, and a plane-wave energy cut-off of 500 eV was used for all simulations. Convergence criteria were set to $1\times10^{-6}$ eV for electronic self-consistent calculations and 0.01 eV/Å for ionic relaxation forces to ensure accuracy. An antiferromagnetic (AFM) spin configuration was applied, with the magnetic moments of Mn atoms initialized in alternating spin orientations. Structural optimization was performed for all materials, allowing full relaxation of lattice parameters and atomic positions. Single-point energy calculations were conducted to obtain structural and electronic properties. The computed results were validated against available experimental data to ensure reliability. Additionally, $Li^+$ diffusion pathways were explored using the bond valence method implemented in the pyAbstantia program.

## 3 Results and discussion

### *3.1 Optimized ground-state structures*

The calculated lattice parameters using the GGA+U method show strong agreement with experimental values, demonstrating the reliability of the approach. For $LiMn_2O_4$, the calculated lattice constant of 8.33 Å slightly overestimates the experimental value of 8.24 Å, resulting in a difference of approximately 1.09%, which falls within the expected range for GGA-based methods. In the case of $Li_2MnO_3$, the computed parameters ($a$ = 4.95 Å, b = 8.54 Å, c = 5.03 Å) closely match the experimental values ($a$ = 4.94 Å, $b$ = 8.53 Å, $c$ = 5.05 Å), with percentage deviations of 0.20%**,** 0.12%, and 0.40%, respectively. The agreement of the lattice parameters of both spinel and layered structures confirms that GGA+U is well-suited for modeling lithium manganese oxides and provides a solid foundation for further property analysis.

| System | Lattice parameters (Å) | |
|---|---|---|
| | GGA+U | Experimental |
| $LiMn_2O_4$ Fd-3m | 8.33 | 8.24 [15] |
| $Li_2MnO_3$ C/2m | $a$=4.95 | $a$=4.94 [16] |
| | $b$=8.54 | $b$=8.53 |
| | $c$=5.03 | $c$=5.05 |

Table 1: Calculated lattice parameters for $LiMn_2O_4$ and $Li_2MnO_3$ using GGA+U.

### *3.2 Mn–O bond lengths*

Figure 2 shows the Mn–O bond environments in $LiMn_2O_4$ and $Li_2MnO_3$. In $LiMn_2O_4$, two types of Mn were identified: $Mn^{3+}$ with longer, distorted Mn–O bonds (up to 2.18 Å), and $Mn^{4+}$ with shorter, more uniform bonds. The distortion around $Mn^{3+}$ is a result of the Jahn–Teller effect, which contributes to structural instability during cycling. In contrast, $Li_2MnO_3$ displays uniform Mn–O bond lengths (~1.91–1.93 Å) consistent with literature values (1.932-1.939 Å) [7], indicating the presence of $Mn^{4+}$ and the absence of distortion. This structural stability suggests that $Li_2MnO_3$ can act as a stabilizing shell, helping to suppress distortion driven degradation in the $LiMn_2O_4$ core.

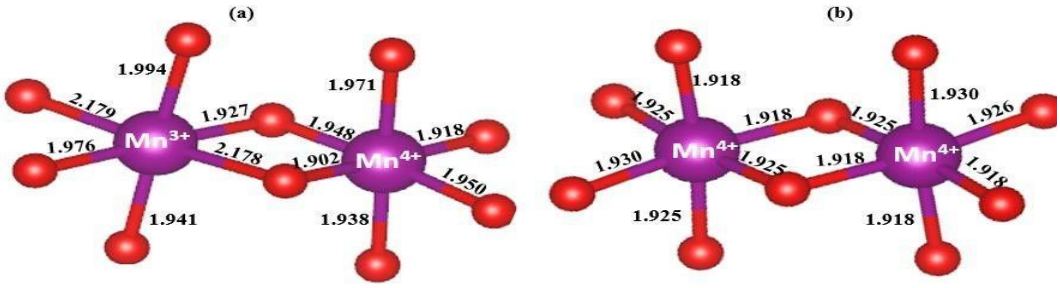


Figure 1: Optimized Mn–O bond environments showing (a) distorted $Mn^{3+}$ and $Mn^{4+}$ octahedra in $LiMn_2O_4$ due to Jahn–Teller effects, and (b) uniform $Mn^{4+}$ coordination in $Li_2MnO_3$.

### *3.3 Magnetic moments*

Table 2 presents the magnetic moments of Mn in both materials to confirm the oxidation states present in $LiMn_2O_4$ and $Li_2MnO_3$. In $LiMn_2O_4$, $Mn^{3+}$ exhibits a higher magnetic moment (~3.8 μB) than $Mn^{4+}$ (~3.0 μB), confirming the presence of mixed-valent states. This mixture contributes to structural issues, as $Mn^{3+}$ is known to cause Jahn–Teller distortion and dissolve into the electrolyte, leading to capacity fading. In contrast, $Li_2MnO_3$ shows consistent magnetic moments around 3.1 μB for all Mn atoms, indicating a uniform $Mn^{4+}$ state. This stable electronic environment enhances $Li_2MnO_3$'s role as an ideal shell material, as it can help suppress the instabilities of $LiMn_2O_4$ and improve the structural and electrochemical performance of the core.

| Material | Valence State | Magnetic Moments (μB) |
|---|---|---|
| $LiMn_2O_4$ | $Mn_{3+}$ | 3.8 |
| | $Mn^{4+}$ | 3.0 |
| $Li_2MnO_3$ | $Mn^{4+}$ | 3.1 |

Table 2: The calculated magnetic moments of Mn in $LiMn_2O_4$ and $Li_2MnO_3$.

### *3.4 Density of states*

The Mn partial density of states (PDOS) for $LiMn_2O_4$ and $Li_2MnO_3$ are shown in Figure 2. In $LiMn_2O_4$, the Mn *d* states approach the Fermi level, resulting in a narrow band gap of approximately 0.5 eV, displaying a semiconducting behaviour. $Li_2MnO_3$ shows a band gap of around 2.1 eV, with no Mn *d* states at the Fermi level. This indicates semiconducting behavior and a $Mn^{4+}$ state. Although its conductivity is low compared to $LiMn_2O_4$, this electronic stability demonstrated by a wider band gap is beneficial in a core–shell configuration. As a shell material, $Li_2MnO_3$ will still allow for conductivity under certain conditions. These band gap values are consistent with experimental reports, validating the accuracy of the electronic structure calculations [17, 18]. These PDOS results support the complementary nature of the two materials: $LiMn_2O_4$ offers electrochemical activity, while $Li_2MnO_3$ provides structural and electronic stability. The wider band gap of $Li_2MnO_3$ further indicates good coating stability but limited electronic conductivity, emphasizing the importance of optimizing its layer thickness. Together, this balance justifies combining the two in a core–shell architecture to enhance overall battery performance.

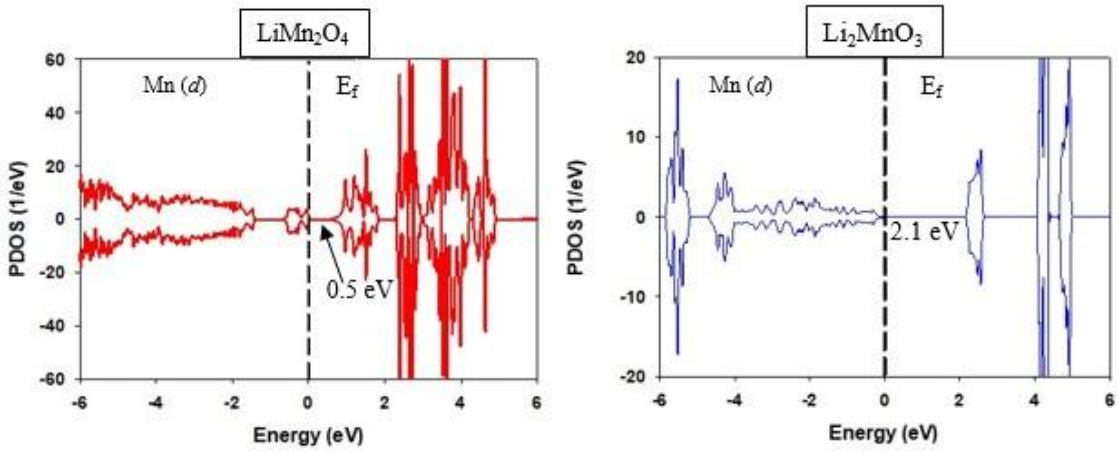


Figure 2: Partial density of states (PDOS) of Mn *d*-orbitals in $LiMn_2O_4$ and $Li_2MnO_3$, showing electronic structure and band gap differences.

### *3.5 Lithium-ion diffusion pathways*

Figure 3 displays the $Li^+$ diffusion pathways in $LiMn_2O_4$ and $Li_2MnO_3$. In $LiMn_2O_4$, lithium ions migrate through a 3D network of channels, enabling fast diffusion and high-rate performance. $Li_2MnO_3$, however, supports lithium transport through a 2D layered pathway. While less open than the 3D framework, this more confined structure offers better control over lithium movement, helping to maintain structural integrity over time. The diffusion pathway analysis helps guide the choice of shell thickness, since the 2D transport in $Li_2MnO_3$ may work better with a thinner shell that matches the faster 3D diffusion in the $LiMn_2O_4$ core, allowing smoother lithium exchange at the interface. The well-ordered layers and uniform $Mn^{4+}$ oxidation state contribute to a more stable and predictable diffusion environment, which is less susceptible to collapse or stress-induced degradation. In the context of a core–shell structure, this makes $Li_2MnO_3$ a valuable shell material. Its 2D diffusion pathway acts as a stabilizing barrier, regulating lithium flow and protecting the high-capacity $LiMn_2O_4$ core from surface degradation.

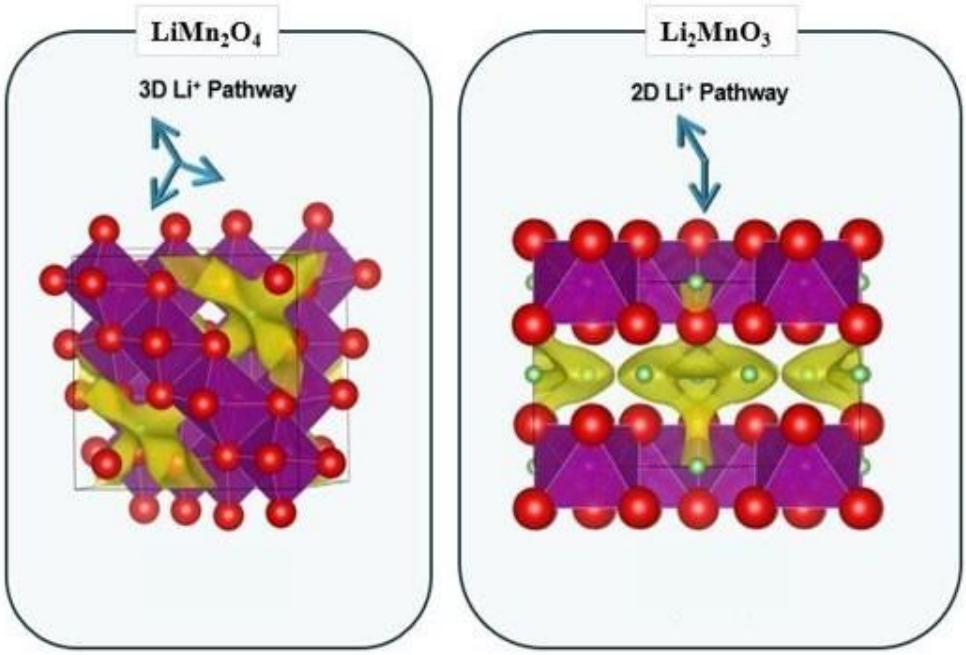


Figure 3: The lithium-ion diffusion pathways: 3D network in spinel $LiMn_2O_4$ vs 2D layered pathways in $Li_2MnO_3$.

## 4 Conclusion

The structural and electronic properties confirm that $LiMn_2O_4$ and $Li_2MnO_3$ have complementary properties that support their use in a core–shell configuration. $LiMn_2O_4$ shows a mixed-valent $Mn^{3+}$/ $Mn^{4+}$ state, a narrow band gap, and a 3D lithium diffusion network, features that contribute to good conductivity and capacity but also cause structural instability due to Jahn–Teller distortion and Mn dissolution. In contrast, $Li_2MnO_3$ is characterized by a stable $Mn^{4+}$ state, a wider semiconducting band gap, and a layered 2D lithium-ion pathway. While its own electronic conductivity and lithium mobility are limited, its structural uniformity and electronic stability make it ideal for surface protection. Together, the results demonstrate that $Li_2MnO_3$ can serve as a stabilizing shell for the $LiMn_2O_4$ core, suppressing surface degradation, enhancing structural durability, and enabling long-term performance. This core–shell combination might offer a strategic balance between electrochemical activity and stability, showing the benefit of $LiMn_2O_4$@$Li_2MnO_3$ as a promising architecture for advanced lithium-ion battery cathodes.

**Acknowledgements**

The authors acknowledge the financial support of the National Research Fund (NRF) and Materials Modelling Centre at the University of Limpopo, as well as the computational resources provided by the National Integrated Cyberinfrastructure System (NICIS).

**References**

[1] J. Ma, T. Liu, J. Ma, C. Zhang, J. Yang, "Progress, Challenge, and Prospect of $LiMnO_2$ : An Adventure toward High-Energy and Low-Cost Li-Ion Batteries," *Advanced Science,* vol. 11, pp. 1-20, 2024.

[2] F. Holtstiege, P. Bärmann, R. Nölle, M. Winter, T. Placke, "Pre-Lithiation Strategies for Rechargeable Energy Storage Technologies: Concepts, Promises and Challenges," *Batteries,* vol. 4, no. 4, pp. 1-39, 2018.

[3] N. M. Jobst, G. Gabrielli, P. Axmann, M. Hölzle, M. Wohlfahrt-Mehrens, "Compensation of the Irreversible Loss of Si-Anodes via Prelithiated NMC/LMO Blend Cathode," *Journal of The Electrochemical Society,* vol. 168, pp. 1-8, 2021.

[4] R. S. Ledwaba, J. C. Womack, C. Skylaris, P. E. Ngoepe, "Intercalation voltages for spinel $Li_xMn_2O_4$ ($0 \leq x \leq 2$) cathode materials: Calibration of calculations with the ONETEP linear-scaling DFT code," *Materials Today Communications,* vol. 27, pp. 1-5, 2021.

[5] G. Tan, S. Wan, J. Chen, H. Yu, Y. Yu, "Reduced Lattice Constant in Al-Doped $LiMn_2O_4$ Nanoparticles for Boosted Electrochemical Lithium Extraction," *Advanced Materials,* vol. 36, pp. 1-10, 2024.

[6] J. Li, B. Zhang, S. Yuan, J. Hou, H. Wu, Y. Huang, W. Han, Z. Feng, Y. Liu, P. Dong, Y. Zhang, Y. Zhang, "Research progress on surface modifcation of spinel $LiMn_2O_4$ cathode materials for lithium-ion batteries," *Ionics,* pp. 1-16, 2025.

[7] M. Michalska, D. A. Buchberger, J. B. Jasinsk, A. K. Thapa, A. Jain, "Surface Modification of Nanocrystalline $LiMn_2O_4$ Using Graphene Oxide Flakes," *Materials,* vol. 12, pp. 1-12, 2021.

[8] S. Tubtimkuna, D. L. Danilov, M. Sawangphruk, P. H. Notten, "Review of the Scalable Core–Shell Synthesis Methods: The Improvements of Li-Ion Battery Electrochemistry and Cycling Stability," *Small Methods,* vol. 7, no. 2300345, 2023.

[9] C. Tomon, S. Sarawutanuku, N. Phattharasupakun, S. Duangdangchote, P. Chomkhuntod, N. Joraleechanchai, P. Bunyanidhi, M. Sawangphruk, "Core-shell structure of $LiMn_2O_4$ cathode material reduces phase transition and Mn dissolution in Li-ion batteries," *Communications Chemistry,* vol. 552, pp. 1-12, 2022.

[10] J. Xu, S. Zhu, Z. Xu, H. Zhu, "The basic physical properties of $Li_2MnO_3$ and $LiMn_2O_4$ cathode materials," *Computational Materials Science,* vol. 229, pp. 1-7, 2023.

[11] W. Kohn, L. J. Sham, "Self-consistent equations including exchangeand correlation effects," *Physical Review,* vol. 140, pp. A1133-A1138, 1965.

[12] G. Kresse, J. Hafner, "Ab initio molecular-dynamics simulation of the liquid-metal–amorphous semiconductor transition in germanium," *Physical Review B,* vol. 49, pp. 14251 - 14269, 1994.

[13] J. P. Perdew, K. Burke, M. Ernzerhof, "Generalized gradient approximation made simple," *Physics Review Letter,* vol. 77, pp. 3865-3868, 1996.

[14] S. L. Dudarev, G. A. Botton, S. Y. Savrasov, C.J. Humphreys, A. P. Sutton, "Electron-energy-loss spectra and the structural stability of nickel oxide: An LSDA+ U study," *Physical Review B,* vol. 57, pp. 1505 - 1509, 1998.

[15] Y. Idemoto, K. Horiko, K. Ui, N. Koura, "Thermodynamic stability and crystal structure dependence of Li content for $Li_xMn_{2-y}M_yO_4$ (M = Mg, A1, Cr, Mn) as a cathode active material for Li secondary battery," *Electrochemistry,* vol. 72, no. 10, pp. 680-687, 2004.

[16] P. Strobel, B. Lambert-Andron, "Crystallographic and magnetic structure of $Li_2MnO_3$," *Journal of solid state chemistry,* vol. 75, pp. 90-98, 1988.

[17] X. Li, J. Wang, S. Zhang, L. Sun, W. Zhang, F. Dang, H. J. Seifert, "Intrinsic Defects in $LiMn_2O_4$: First Principles Calculations," *ACS Omega,* vol. 6, p. 21255−21264, 2021.

[18] R. Xiao, H. Li, L. Chen, "Density Functional Investigation on $Li_2MnO_3$," *Chemical Material,* vol. 24, p. 4242−4251, 2012.

This page intentionally left blank.